NANOSYSTEMS: PHYSICS, CHEMISTRY, MATHEMATICS, 2019, 10 (3), P. 282–288

Composite membranes based on geometrically constrained PIM-1 for dehumidification of gas mixtures

E. A. Chernova, I. V. Roslyakov, S. G. Dorofeev, A. V. Lukashin

Lomonosov Moscow State University, Leninskiye Gory, Moscow, 119991, Russia

wellastra@gmail.com, alexey.lukashin@gmail.com

PACS 81.05.Rm, 47.56.+r **DOI 10.17586/2220-8054-2019-10-3-282-288**

Composite membranes based on polymer with intrinsic microporosity (PIM-1) confined in the pores of porous anodic alumina (AAO) supports were prepared by spin-coating method under vacuum suction. Water permeance of the membranes was measured at humidities ranging from 10 to 70 %. High permeance towards water vapors reaching the value of $\sim$ 13700 l/(m^2·bar·h) coupled with the H_2O/N_2 selectivity of 1400 was observed at the humidity of 70 % for composite membranes due to the condensation in nanopores of polymer and anodic alumina channels. The obtained selectivity exceeds strongly that of bulk PIM-1 due to confinement of polymer chains mobility in AAO channels. The water vapor sorption capacity for composite membranes exceeds 7 % being governed both by condensation in polymer micropores and anodic alumina channels. Physical ageing of the membranes was monitored for a period of 6 months and then the membranes were subjected to activation in methanol. It was established that physical ageing substantially reduces the water permeance but activation in methanol allows one to partially rejuvenate water transport performance.

Keywords: dehumidification, polymer with intrinsic microporosity, geometric confinement, physical ageing.

Received: 16 May 2019

Revised: 25 May 2019

1. Introduction

Dehumidification of gas mixtures is of vital importance in industry, including natural gas purification in the petroleum industry and air conditioning for electronics, food industry and medicine [1]. For this purpose, membrane technology is of great demand, owing to its low cost and high performance [2–4]. Among membrane separation technologies, capillary transport of water vapor appears favorable as providing both high permeance and selectivity due to the blockage of membrane channels by the condensate. Membrane operation in the capillary transport regime has been previously reported for inorganic membranes, including Vycor glass [5], porous anodic alumina [6, 7], graphene oxide [8, 9], as well as microporous polymer membranes with thermodynamic (reverse) selectivity, including polysulfone, sulfonated polyether-etherketon (sPEEK) and poly-trimethylsylilpropyne (PTMSP) [10, 11]. Due to high solubility of water vapors in hydrophilic microporous polymers, it becomes possible to achieve outstanding membrane performance. Among the listed polymers, the highest permeance of 61000 Barrer coupled with high H_2O/N_2 selectivity of 10^7 is exhibited by sulfonated polyether-etherketone [12]. On the other hand, polymer membranes are easily degradable due to the plasticization in the presence of water vapor; also, high H_2O sorption capacity usually demands a means of polymer regeneration. Another drawback is the implementation of bulk polymer membranes which are rather expensive. Thus, there is still a need for high-quality mechanically stable membranes for the dehumidification of gases.

A good decision is the design of composite polymer-inorganic membranes where the mechanically-stable highly-permeable support provides the robustness of the membrane, while the polymer thin selective layer provides high performance and selectivity. Recently, we have shown that geometric confinement of polymer chains in a rigid matrix can strongly hinder the transport of permanent gases [13, 14]. As a result, polymers confined in nanochannels illustrate significant reduction of permeance towards permanent gases, whereas the transport characteristics of condensable vapors are preserved due to polymer swelling. The effect enhances polymer selectivity, and is best pronounced for rigid polymers with large Kuhn segment. A good candidate for this purpose is polymer with intrinsic microporosity (PIM-1) with rigid ladder-like macromolecules and the size of Kuhn segment equal to the entire size of the macromolecule. Also, owing to the polar nature of its monomer unit due to the presence of nitrile groups and ether oxygen, PIM-1 exhibits elevated sorption capacity towards water vapor [4].

In the present paper, we apply the concept of geometric confinement to the preparation of PIM-1-based composite membranes for the dehumidification of gases. The composite membranes were obtained by spin-coating onto nanoporous anodic aluminum oxide (AAO) supports, their permeance and sorption capacity towards water vapors was

measured, the evolution of permeance and selectivity was monitored in time and the influence of membrane activation with methanol was tested.

2. Experimental section

Anodic alumina films, utilized as membrane supports, were prepared by anodic oxidation of high purity aluminum in 0.3 M oxalic acid at 40 V and in 0.3 M sulfuric acid at 25V. The detailed description of the AAO preparation can be found in [15–17]. Composite membranes were obtained by spin-coating of 1 wt.% polymer solution in chloroform onto AAO supports under vacuum suction. Detailed preparation procedure is described in [15].

The microstructure of AAO supports and composite membranes was studied using SEM Carl Zeiss NVision 40 (5 kV, InLens detector) electron microscope. The homogeneity of PIM-1 layer of composite membranes was examined with luminescence microscopy on Renishaw InVia spectrometer equipped with Leica DMLM optics (50× objective) with 20 mW 514 nm Ar laser excitation. Luminescence intensity distribution maps were acquired in streamline mode with line-focused laser beam (a length of ~ 50 μm and a thickness below 1 μm) with point accumulation time of 10 s. The obtained intensity distribution maps were treated in Wire 3.4 Renishaw software.

Sorption capacity towards H_2O for composite membrane PIM-1/AAO-40, AAO-40 membrane and PIM-1 thin film, was measured using quartz microbalance. The outer selective layer of the PIM-1/AAO-40 sample was preliminary removed using wipe with chloroform so that the sample include only geometrically-confined polymer. Then, composite membranes as well as AAO-40 membrane, were grinded into a fine powder and deposited onto both sides of the quartz resonators with the fundamental frequency of 12 MHz. PIM-1 polymer thin film was deposited on the surface of the quartz resonators from 0.05 wt.% solution in chloroform. Typical frequency shift after sample deposition was ~ 30 kHz. The change of frequency of quartz resonators upon sorption of water vapors was calculated as follows:

$$\omega\,(\mathrm{H_2O}) = \frac{\Delta f\,(\mathrm{H_2O}) - \Delta f_0 - f_0}{\Delta f_0} \cdot 100\ \%,$$

where $\omega\,(\mathrm{H_2O})$ – water sorption capacity of the sample, %, Δf_0 – frequency shift of quartz resonator with deposited sample at zero humidity, MHz, $\Delta f\,(\mathrm{H_2O})$ – frequency shift of quartz resonator with deposited sample during the sorption of water, MHz.

The permeance of AAO supports and composite membranes was measured in two-compartment cross-flow cell using a permeance setup equipped with SLA5850 mass-flow controllers (Brooks, England), PD-100-DI pressure transducers (OVEN, Russia) and T-Station 75 vacuum system (BOC Edwards, England). The gas scheme of experimental setup has been described recently in [8]. The measurements were performed at ambient temperature (22 ± 2 °C). The flux and humidity of air was controlled with two mass-flow controllers SLA5850 (Brooks, USA). To control the humidity one of inlet air streams was saturated with water vapor in humidifier by direct air-water contact. Air temperature and humidity on the inlet and outlet of a composite membrane was monitored by HIH-4000 (Honeywell, USA) sensors. Dew point temperature of the outlet air was also determined by a chilled mirror dew-point hygrometer TOROS-3VY (Ukraine). The permeance of water was calculated using the following equation:

$$F = \frac{J(\mathrm{He}) \cdot RH_{out}}{S \cdot P_{sat} \cdot (RH_{in} - RH_{out})},$$

where $J(\mathrm{He})$ – helium carrier flux, RH_{in} and RH_{out} – inlet and outlet relative humidity, P_{sat} – saturated water vapor pressure at a given temperature (calculation was performed by Antoinie Equation with coefficients determined by Stull [18]), and S – membrane area.

3. Results and discussion

According to SEM, the microstructure of the composite membranes comprises a few m-thick dense outer layer and porous AAO support with partly infilled pores (Fig. 1). The thickness of the external polymer selective layer is somewhat lower for PIM-1/AAO-40 membrane which can result from more effective infiltration of macromolecules (Table 1). The inner selective layer is represented by polymer nanofibers formed during infiltration of polymer solution into the AAO channels. The polymer replica obtained from the PIM-1/AAO-40 sample after the dissolution of the AAO support in 0.3 V NaOH, clearly evidences the formation of partly hollow polymer fibers and directly proves the polymer infiltration into the AAO supports.

To prove the uniformity of the polymer selective layers and quantify the amount of polymer in composite membranes, the maps of polymer luminescence intensity were recorded (Fig. 2). As it has been shown recently, the photoluminescence (PL) intensity of thin PIM-1 films can be used as semiquantitative characteristics of PIM-1 content [14].

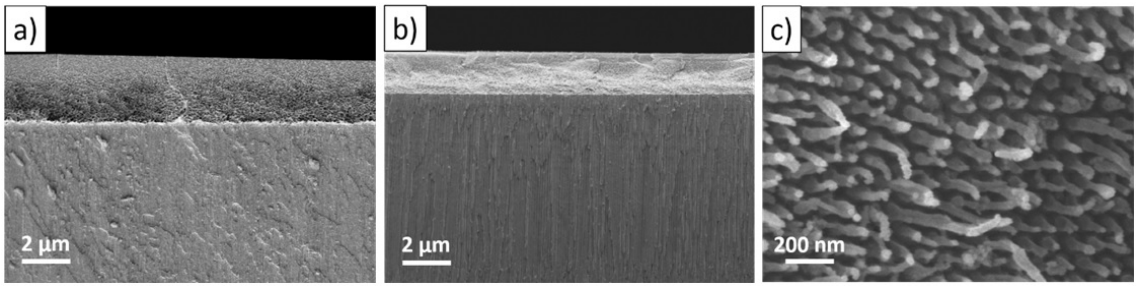

FIG. 1. SEM-images of composite membranes: a) cross-section of PIM-1/AAO-25 membrane; b) cross-section of PIM-1/AAO-40 membrane; c) polymer replica of the selective layer of PIM-1/AAO-40 membrane

TABLE 1. Microstructure characteristics and statistical analysis of luminescence intensity maps for PIM-1-based composite membranes

Sample	Thickness of the external selective layer (SEM), μm	Pore diameter of the AAO support, nm	Average PL intensity, cps·10^4	PL intensity RSD, %	PL intensity interval for P_{90}, cps·10^4
PIM-1/AAO-25	2.6 ± 0.1	21 ± 5	2.82	10.2	2.44 – 3.41
PIM-1/AAO-40	2.0 ± 0.1	36 ± 5	3.50	5.77	3.16 – 3.81

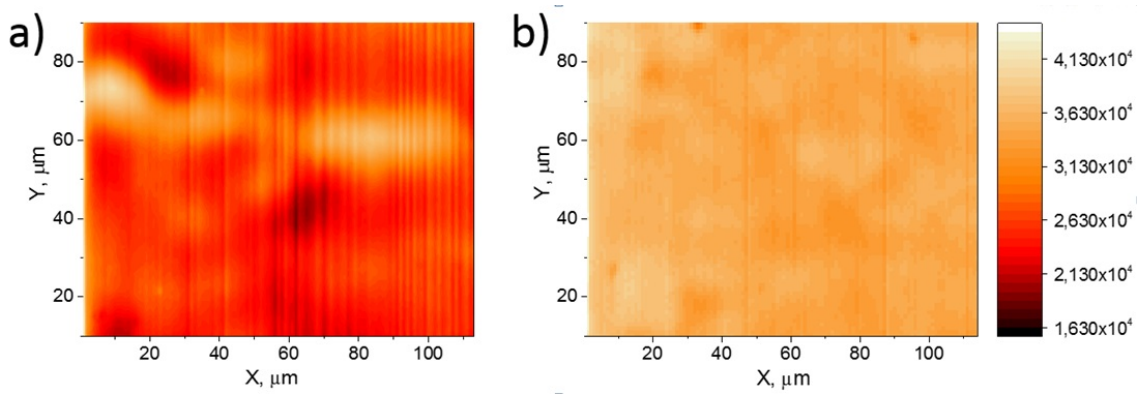

FIG. 2. Luminescence intensity distribution maps for a) PIM-1/AAO-25; b) PIM-1/AAO-40 membranes

According to the obtained results, the luminescence intensity is uniform enough across the whole thickness of the selective coatings indicating polymer macromolecules are homogeneously distributed on the surface of the AAO support. The statistical analysis has shown (Table 1) that the relative standard deviation (RSD) of luminescence intensity along the membrane for PIM-1/AAO-25 sample is nearly 2 times higher than for PIM-1/AAO-40 sample, indicating more uneven distribution of macromolecules in PIM-1/AAO-25 which also can be associated with hindrances of macromolecules incorporation into small-diameter nanochannels. Note that the average luminescence intensity of the PIM-1/AAO-40 sample is greater as compared to the PIM-1/AAO-25 membrane, while the thickness of the external layer for this sample is smaller (see Table 1). This suggests that the greater quantity of the polymer is introduced into AAO under vacuum suction for the substrate with larger diameter of the channels. This stays in line with increasing liquid permeance of AAO membranes with pore diameters [17].

To get detailed understanding of water vapor transport in composite membranes, the sorption capacity of PIM-1/AAO-40 sample as well as anodic alumina AAO-40 and pure PIM-1 thin film was measured as a function of partial water vapor pressure using quartz microbalance method (Fig. 3).

According to the obtained results, all the isotherms include 3 standard regions: the Henry region (up to 0.3 P_0), the Langmuir region (0.3 – 0.6 P_0) and the region of capillary condensation (over 0.6 P_0).

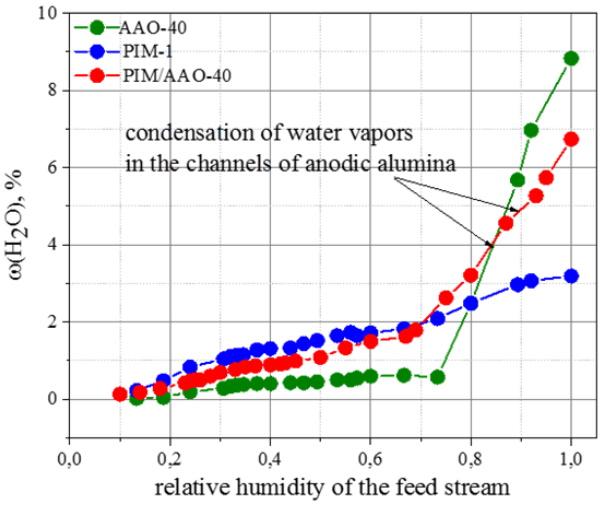

FIG. 3. Sorption isotherms of water vapor on the composite membrane PIM-1/AAO-40, anodic alumina AAO-40 and thin PIM-1 polymer film

A significant increase in sorption capacity of the AAO-40 substrate is observed at the humidity of 75 % which can be attributed to the capillary condensation of water vapor in nanometer-sized channels of the AAO [7, 19, 20]. According to the Kelvin equation, the capillary radius can be estimated as:

$$r = \frac{2\sigma M}{\rho RT \cdot \ln\left(p_c/p_0\right)},$$

where σ is the surface tension of liquid water, p_c and p_0 are the pressure of condensation in the pore with radius r and the pressure of water vapors condensation on a flat surface, respectively, M and ρ are the molecular mass and density of water.

Taking the beginning of the capillary condensation in the AAO-40 film at the relative pressure of 0.75 P_0, the condensation diameter can be estimated as 7.4 nm which differs dramatically from the diameter of AAO channels ($\sim 35 \pm 5$ nm). The value can be attributed to the presence of small-sized mesopores in AAO walls, accessible to the condensation of water, those were evidenced during examination of thermal properties of AAO membranes [21].

The sample of PIM-1 polymer exhibits maximal sorption capacity of 3.2 % manifesting the filling of polymer free volume elements with water molecules. At $\sim$ 0.4 P_0, the first kink at the isotherm is observed, corresponding likely to beginning of filling of free-volume elements with water molecules. The average diameter of the microvoids in PIM-1 according to the Kelvin equation was estimated as 4 nm. According to the data obtained from NMR, PALS, and low-temperature nitrogen adsorption, the average diameter of spherical microvoids in PIM-1 polymer ranges from 0.6 to 1 nm [22,23]. The discrepancy in the derived values can be regarded to some variation of the accessible porosity in PIM-1 for water vapors, governed by hydrophilicity of polymer and its local structure [4].

The sorption capacity of PIM-1/AAO-40 sample can be regarded as a result of cooperative sorption in the AAO-40 matrix and the PIM-1 polymer. In the range 0.1 – 0.7 P_0 it follows the behavior of the PIM-1 sorption curve, while at $\sim$ 0.7 P_0 the in-channel condensation of water vapors begins. At low humidity range the sorption curve for the PIM-1/AAO-40 is located significantly higher than that for the AAO-40 substrate, suggesting that the sorption of water vapors is provided mainly by the polymer inside the AAO channels. Besides, the condensation in PIM-1/AAO-40 composite membrane begins at lower pressure compared to AAO-40 support which can be attributed to the facilitated condensation in the free volume elements generated by polymer in the AAO pores. Thus, the porosity, available for water condensation in composite membrane inherits both the features of PIM-1 and AAO, while high enough H_2O vapor sorption capacity allows their application in dehumidification processes.

Figure 4 (a, b) represents the dependencies of water vapor permeance on the humidity of the feed stream for PIM-1/AAO-25 and PIM-1/AAO-40 composite membranes, respectively. An increase in permeance with the elevation of humidity level is observed owing to the growth of the sorption capacity. At a humidity of 70 %, the maximum permeance value of 19000 L/(m^2·bar·h) is achieved for the membrane PIM-1/AAO-40 accompanied with the H_2O/N_2 selectivity of 600 (Table 2). The permeance of the PIM-1/AAO-25 composite membrane is lower (13700 L/(m^2·bar·h), due to the smaller channels of the AAO-25 support which hinder polymer chains mobility and elevates the vapors flow resistance. This effect allows one to reach greater H_2O/N_2 selectivity for PIM-1/AAO-25 (see Table 2). The maximum

membrane selectivity of 1400 is achieved for the PIM-1/AAO-25 composite membrane at the feed humidity of 70 % which, coupled with the high permeance, is favorable for air dehumidification processes.

According to Fig. 4, the significant reduction of permeance of composite membranes is observed with time which can be attributed to the physical ageing of polymer structure. To quantitatively show the decay of the membrane permeance, the permeance reduction coefficient was calculated P^L (see Table 2):

$$P^L = \frac{P_{ref} - P_C}{P_{ref}} \cdot 100\ \%,$$

where P_C – the permeance of composite membrane under physical ageing, L/(m^2·bar·h), P_{ref} – the permance of freshly prepared membrane, L/(m^2·bar·h).

TABLE 2. The permeance, ideal selectivity and permeance reduction coefficients for the PIM-1-based composite membranes at the feed flow humidity of 70 %

Sample	Permeance, L/(m^2·bar·h)		Selectivity H_2O/N_2	Permeance reduction coefficients at the humidity of 70 %, %
	H_2O	N_2		
PIM-1, bulk 50 μm [4]	**1590**	**20**	**80**	**—**
PIM-1/AAO-25	**13700**	**10**	**1400**	**—**
PIM-1/AAO-25-2m	9700	7	1390	30
PIM-1/AAO-25-6m	3100	4	770	80
PIM-1/AAO-25-6m-CH_3OH	9970	30	330	30
PIM-1/AAO-40	**19000**	**30**	**600**	**—**
PIM-1/AAO-40-2m	10100	20	500	50
PIM-1/AAO-40-6m	4020	9	450	80
PIM-1/AAO-40-6m-CH_3OH	15250	40	400	25

During the first two months of physical ageing, composite membranes lose about 30 – 50 % of the initial permeance, and after 6 months, the permeance reduction achieves $\sim$ 80 % manifesting the significant compaction of selective polymer layers due to the relaxation of macromolecules to thermodynamically stable conformations (Table 2). The accelerated reduction of polymer permeance can be associated with the effect of geometric confinement in the channels of AAO. Nevertheless, the H_2O/N_2 selectivity of physically-aged composite membranes stays nearly at the same level due to the synchronous reduction of polymer permeance towards water vapors as well as N_2. At the same time, the significant fall in permeance discounts this virtue.

It is well documented that the soaking of microporous polymers in methanol and ethanol can be considered as one of the ways to rejuvenate the polymer permeance [24,25]. The specific interactions of alcohol molecules with polymer chains leads to the enhancement of local segmental mobility of the macromolecules and the most pronounced effect is observed when methanol is used. In this work, the composite membranes were activated by soaking in pure methanol for a few minutes. According to Fig. 4, the activation in methanol enables one to elevate the membrane permeance, but it does not allow one to reach the initial permeance level of fresh membranes. For activated PIM-1/AAO-25 and PIM-1/AAO-40 composite membranes, the water permeance achieves the values of 80 % of the initial permeances for freshly-prepared membranes. According to [26] and [4], water molecules can form stable water clusters inside the free-volume elements of the polymer which can hardly be removed from the structure. This phenomenon can be considered as one of the key reasons preventing the complete rejuvenation of polymer permeance during activation. Nevertheless, the achieved regeneration values can be considered as high enough for practical applications.

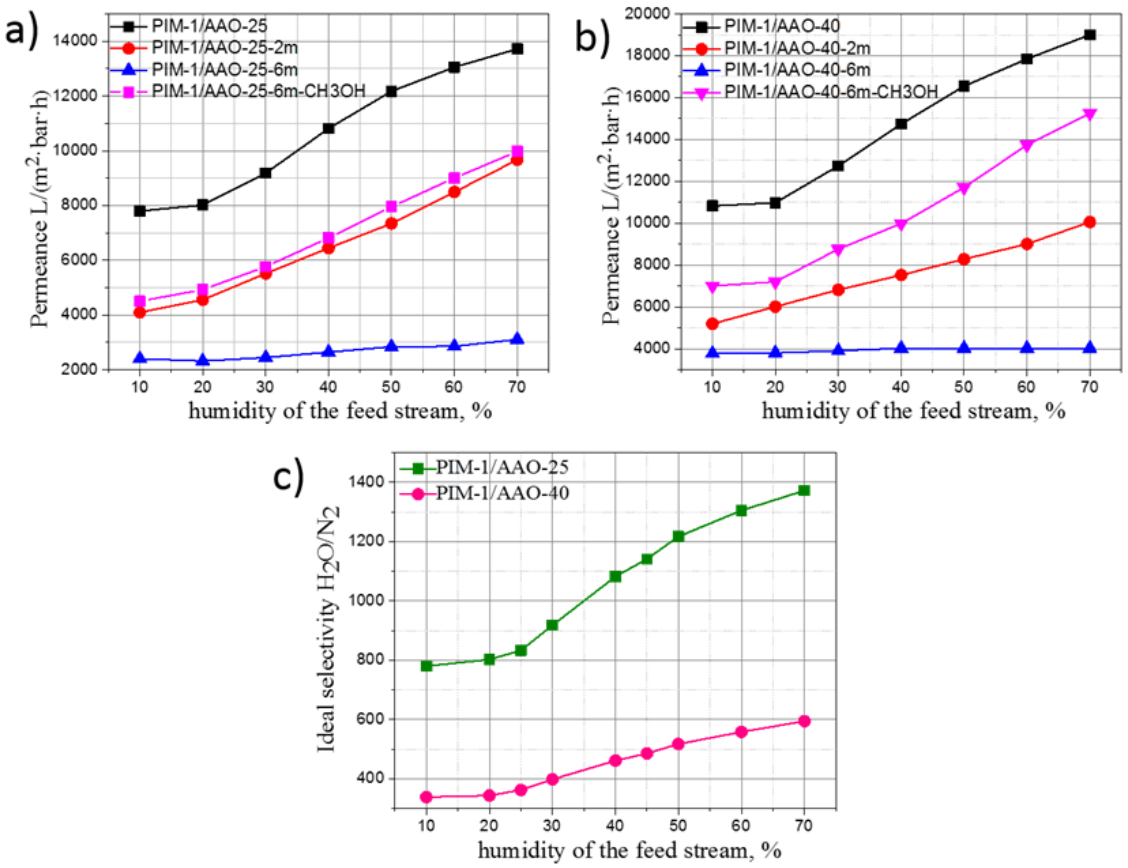

FIG. 4. The dependence of water vapor permeance on relative humidity of the feed gas for the composite membranes:) PIM-1/AAO-25; b) PIM-1/AAO-40; c) the dependence of H_2O/N_2 selectivity of composite membranes on the humidity of the feed gas for the freshly-prepared membranes

4. Conclusions

Thus, composite membranes based on polymer with intrinsic microporosity (PIM-1) spatially confined in the pores of anodic alumina membranes with variable diameter have been considered as potential material for gas dehumidification processes. The H_2O vapors sorption capacity of the composite membranes was found to be a result of the cooperative sorption in PIM-1 polymer and AAO support with the dominating role of PIM-1 in the water vapor transport. It is shown that for the freshly-prepared PIM-1-based composite membranes the H_2O vapor permeance increases strongly with humidity, owing to the polar nature of the PIM-1. On the other hand, the confined polymeric phase exhibits strong hindrance for permanent gases transport giving rise to the enhancement of H_2O/N_2 ideal selectivity up to 1400 compared to bulk polymer selectivity of 80. During 6 months of physical ageing, composite membranes lose about 80 % of their initial H_2O vapor permeance accompanied by loss in selectivity. The activation in methanol allows to rejuvenate up to 80 % of the initial polymer permeance. According to the obtained results, PIM-1-based composite membranes are suitable candidates for water vapor extraction from gas streams, but regular activation in methanol is required in order to save optimal polymer performance.

Acknowledgements

The authors are grateful to A. A. Eliseev and D. I. Petukhov (Lomonosov Moscow State University) for the help in experimental work and discussion of the results. The work is supported by the Ministry of education and science of the Russian Federation within a Federal Targeted Programme for "Research and Development in Priority Areas of Development of the Russian Scientific and Technological Complex for 2014–2020" (Agreement No. 14.604.21.0177, unique Project Identification RFMEFI60417X0177).

References

[1] Yang B., Weixing Y., Gao F., Guo B. A review of membrane-based air dehumidification. *Indoor and Built Environment*, 2013, **24** (1), P. 11–26.

[2] Baker R.W., Low B.T. Gas separation membrane materials: A perspective. *Macromolecules*, 2014, **47** (20), P. 6999–7013.

[3] Sadilov I.S., Petukhov D.I., Eliseev A.A. Enhancing gas separation efficiency by surface functionalization of nanoporous membranes. *Separation and Purification Technology*, 2019, **221**, P. 74–82.

[4] Scholes C.A., Jin J., Stevens G.W., Kentish S.E. Competitive permeation of gas and water vapour in high free volume polymeric membranes. *Journal of Polymer Science Part B: Polymer Physics*, 2015, **53** (10), P. 719–728.

[5] Uchytil P., Petrickovic R., Seidel-Morgenstern A. Study of capillary condensation of butane in a Vycor glass membrane. *Journal of Membrane Science*, 2005, **64** (1–2), P. 27–36.

[6] Lira H. de L., Paterson R. New and modified anodic alumina membranes: Part III. Preparation and characterisation by gas diffusion of 5 nm pore size anodic alumina membranes. *Journal of Membrane Science*, 2002, **206** (1–2), P. 375–387.

[7] Petukhov D.I., Berekchiian M.V., Eliseev A.A. Meniscus Curvature Effect on the Asymmetric Mass Transport through Nanochannels in Capillary Condensation Regime. *The Journal of Physical Chemistry C*, 2018, **122** (51), P. 29537–29548.

[8] Petukhov D.I., Chernova E.A., et al. Thin graphene oxide membranes for gas dehumidification. *Journal of Membrane Science*, 2018, **577**, P. 184–194.

[9] Eliseev An.A., Poyarkov A.A., et al. Operando study of water vapor transport through ultra-thin graphene oxide membranes. *2D Materials*, 2019, **6** (3), 035039.

[10] Bolto B., Hoang M., Xie Z. A review of water recovery by vapour permeation through membranes. *Water Research*, 2012, **46** (2), P. 259–266.

[11] Metz S.J., van De Ven W.J.C., et al. Transport of water vapor and inert gas mixtures through highly selective and highly permeable polymer membranes. *Journal of Membrane Science*, 2005, **251** (1–2), P. 29–41.

[12] Shengzhou L., Feng W., Tianlu C. Synthesis of Poly(ether ether ketone)s with High Content of Sodium Sulfonate Groups as Gas Dehumidification Membrane Materials. *Macromolecular Rapid Communications*, 2001, **22** (8), P. 579–582.

[13] Chernova E.A., Bermeshev M.A., et al. The effect of geometric confinement on gas separation characteristics of additive poly[3-(trimethylsilyl)tricyclononene-7]. *Nanosystems: Physics, Chemistry, Mathematics*, 2018, **9** (2), P. 252–258.

[14] Chernova E., Petukhov D., et al. Enhanced gas separation factors of microporous polymer constrained in the channels of anodic alumina membranes. *Scientific Reports*, 2016, **6**, P. 31183.

[15] Petukhov D.I., Napolskii K.S., et al. Comparative study of structure and permeability of porous oxide films on aluminum obtained by single- and two-step anodization. *ACS Applied Materials and Interfaces*, 2013, **5** (16), P. 7819–7824.

[16] Petukhov D.I., Napolskii K.S., Eliseev A.A. Permeability of anodic alumina membranes with branched channels. *Nanotechnology*, 2012, **23** (33), P. 335601.

[17] Petukhov D.I., Buldakov D.A., et al. Liquid permeation and chemical stability of anodic alumina membranes. *Beilstein Journal of Nanotechnology*, 2017, **8**, P. 561–570.

[18] Stull D.R. Vapor Pressure of Pure Substances. Organic and Inorganic Compounds. *Industrial & Engineering Chemistry*, 1947, **39** (4), P. 517–540.

[19] Petukhov D.I., Berekchiian M.V., et al. Experimental and Theoretical Study of Enhanced Vapor Transport through Nanochannels of Anodic Alumina Membranes in a Capillary Condensation Regime. *The Journal of Physical Chemistry C*, 2016, **120** (20), P. 10982–10990.

[20] Petukhov D.I., Eliseev A.A. Gas permeation through nanoporous membranes in the transitional flow region. *Nanotechnology*, 2016, **27** (8), P. 85707.

[21] Roslyakov I.V., Napolskii K.S., et al. Thermal properties of anodic alumina membranes. *Nanosystems: Physics, Chemistry, Mathematics*, 2013, **4** (1), P. 120–129.

[22] Emmler T., Heinrich K., et al. Free Volume Investigation of Polymers of Intrinsic Microporosity (PIMs): PIM-1 and PIM1 Copolymers Incorporating Ethanoanthracene Units. *Macromolecules*, 2010, **43** (14), P. 6075–6084.

[23] Shantarovich V.P., Suzuki T., et al. Structural heterogeneity in glassy polymeric materials revealed by positron annihilation and other supplementary techniques. *Physica status solidi*, 2007, **4** (10), P. 3776–3779.

[24] Chaukura N. Interaction of a Polymer of Intrinsic Microporosity (PIM-1) with Penetrants. *American Journal of Applied Chemistry*, 2015, **3** (3), P. 139.

[25] Yampolskii Y., Alentiev A., et al. Intermolecular Interactions: New Way to Govern Transport Properties of Membrane Materials. *Industrial & Engineering Chemistry Research*, 2010, **49** (23), P. 12031–12037.

[26] Lasseuguette E., Ferrari M.-C., Brandani S. Humidity Impact on the Gas Permeability of PIM-1 Membrane for Post-combustion Application. *Energy Procedia*, 2014, **63**, P. 194–201.